Diamond Based DDR IMPATTs: Prospects and Potentiality as Millimeter-Wave Source at 94 GHz Atmospheric Window

Aritra ACHARYYA [1], *Koyel DATTA* [2], *Raya GHOSH* [2], *Monalisa SARKAR* [2],
Roshmy SANYAL [2], *Suranjana BANERJEE* [3], *J. P. BANERJEE* [1]

[1] Inst. of Radio Physics and Electronics, University of Calcutta, 92, APC Road, Kolkata 700009, India
[2] Supreme Knowledge Foundation Group of Institutions, Sir J. C. Bose School of Engineering, 1, Khan Road, Mankundu, Hooghly, West Bengal 712139, India
[3] Academy of Technology, West Bengal University of Technology, Adisaptagram, Hooghly 712121, West Bengal, India

ari_besu@yahoo.co.in, k.datta10@yahoo.in, rayaghosh86@gmail.com, mona.wpc@gmail.com,
roshmysanyal09@gmail.com, suranjanarpe21@yahoo.com, jpbanerjee06@rediffmail.com

Abstract. *Large-signal simulation is carried out in this paper to investigate the prospects and potentiality of Double-Drift Region (DDR) Impact Avalanche Transit Time (IMPATT) device based on semiconducting type-IIb diamond as millimeter-wave source operating at 94 GHz atmospheric window frequency. Large-signal simulation method developed by the authors and presented in this paper is based on non-sinusoidal voltage excitation. The simulation is carried out to obtain the large-signal characteristics such as RF power output, DC to RF conversion efficiency etc. of DDR diamond IMPATT device designed to operate at 94 GHz. The results show that the device is capable of delivering a peak RF power output of 7.01 W with 10.18% DC to RF conversion efficiency for a bias current density of* 6.0×10^{8} *Am*$^{-2}$ *and voltage modulation of 60% at 94 GHz; whereas for the same voltage modulation 94 GHz DDR Si IMPATT can deliver only 693.82 mW RF power with 8.74 efficiency for the bias current density of* 3.4×10^{8} *Am*$^{-2}$.

Keywords

Diamond, DDR IMPATTs, large-signal simulation, millimeter-wave.

1. Introduction

The electronic, optical, mechanical and thermal properties of semiconducting type-IIb diamond having 5.48 eV bandgap and the recent development of its epitaxial growth technique have aroused a lot of interest to use this material for fabrication of high power, high frequency semiconductor devices. Prospects of diamond (C) based electronic devices such as Metal Semiconductor Field-Effect Transistor (MESFET), IMPATT diode and Bipolar Junction Transistor (BJT) for microwave and mm-wave power generation was studied by Trew et al. [1] in 1991. Impact Avalanche Transit Time (IMPATT) devices are well established as high power, high efficiency solid-state sources at microwave (3-30 GHz) and millimeter-wave (30 to 300 GHz) frequency bands [2]-[4]. In the decades of seventies, Si and GaAs were mostly used as base materials for IMPATT diodes [5]-[10]. In recent years IMPATT diodes based on wide bandgap (WBG) semiconductor materials (SiC, GaN) have been reported for generation of RF power at mm-wave and terahertz frequencies [11]-[19]. Material properties of diamond are also suitable for fabrication of IMPATT diodes at mm-wave frequencies [20]-[24]. This fact influenced the authors to study the millimeter-wave properties of DDR IMPATTs based on diamond at 94 GHz atmospheric window to explore its potentiality as possible mm-wave source. In the present paper, the large-signal simulation based on non-sinusoidal voltage excitation model [25]-[28] is carried out to investigate the large-signal properties of DDR IMPATT device based on type-IIb diamond designed to operate at 94 GHz. The large-signal parameters such as RF power output, DC to RF conversion efficiency, negative conductance, susceptance, optimum frequency, avalanche resonance frequency etc. of the device are obtained from the simulation. These results are compared with the simulation results of conventional DDR Si IMPATT operating at 94 GHz to ensure the superiority of diamond as semiconductor base material of IMPATT devices.

2. Large-Signal Modeling and Simulation Technique

One-dimensional model of reverse biased n^{+}-n-p-p^{+} structure of DDR IMPATT device, shown in Fig. 1 (a) is used for large-signal simulation since the physical phenomena take place in the semiconductor bulk along the symmetry axis of the mesa structure of the device. The fundamental time and space dependent device equations i.e., Poisson's equation, continuity equations, current density equations involving mobile space charge are simultaneously solved under large-signal condition subject to suitable boundary conditions to obtain the snap-shots of electric field $\xi(x,t)$ and normalized current density $P(x,t) = (J_p(x,t) - J_n(x,t))/J_0(t)$; where $J_0(t) = J_p(x,t) + J_n(x,t)$ for different bias current densities at several instants of time of one complete cycle of steady-state oscillation. The large-signal simulation [25]-[28] is carried out by considering 500 space steps and 150 time steps. In the present simulation method, the IMPATT device is considered as a non-sinusoidal voltage driven source as shown in Fig. 1 (b). The input AC voltage is taken as

$$V_{RF}(t) = V_B \sum_{p=1}^{n} m_x{}^p \, sin(p\omega t) \tag{1}$$

where V_{RF} is the RF voltage, V_B is the breakdown voltage of the device, m_x is the voltage modulation factor and ω is the angular frequency. The bias voltage is applied through a coupling capacitor C to study the performance of the device at a given fundamental frequency $f = \omega/2\pi$ with its n harmonics.

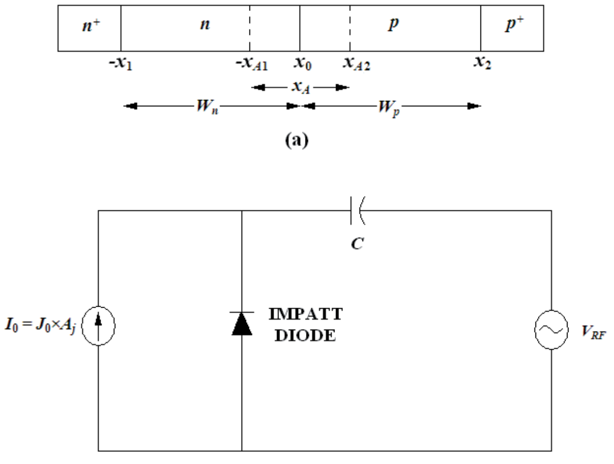

(a)

(b)

Fig. 1. (a) One-dimensional model of DDR IMPATT device, (b) voltage driven IMPATT oscillator and associated circuit.

The large-signal program [25]-[28] is run till the limit of one complete cycle (i.e. $0 \leq \omega t \leq 2\pi$) is reached. The bias current density, RF voltage amplitude and frequency are J_0, V_{RF} and f respectively. The terminal current and voltage waveforms for a complete cycle of oscillation are analyzed to study the RF performance of the device at different phase angles of one complete cycle of oscillation i.e., $\omega t = 0, \pi/2, \pi, 3\pi/2, 2\pi$.

3. Results and Discussion

The active layer widths (W_n, W_p) and background doping concentrations (N_D, N_A) of 94 GHz DDR diamond IMPATT are initially chosen by using the transit time formula of Sze and Ryder [29]. The structural and doping parameters of the device are designed for optimum performance at 94 GHz by using the method described in earlier paper [25]. The doping concentrations of n^+- and p^+-layers (N_{n+} and N_{p+}) are taken in the order of ~10^{25} m^{-3} in the simulation. Structural and doping parameters of the designed DDR diamond IMPATT device are given in Tab. 1. The realistic field dependence of ionization rates (α_n, α_p), drift velocities (v_n, v_p) of charge carriers and other material parameters such as bandgap (E_g), intrinsic carrier concentration (n_i), effective density of states of conduction and valance bands (N_c, N_v), diffusion coefficients (D_n, D_p), mobilities (μ_n, μ_p) and diffusion lengths (L_n, L_p) of diamond are taken from the recently published experimental reports [30]-[35]. Junction diameter of the device (D_j) is taken as 35 μm for continuous-wave (CW) operation at 94 GHz [5], [6].

DESIGN PARAMETER	VALUE
f_d (GHz)	94
W_n (μm)	0.795
W_p (μm)	0.790
N_D (×10^{23} m^{-3})	0.460
N_A (×10^{23} m^{-3})	0.530
N_{n+} (×10^{25} m^{-3})	5.000
N_{p+} (×10^{25} m^{-3})	2.700

Tab 1. Structural and doping parameters.

3.1 Static Properties

Bias current density (J_0) is varied from 3.0×10^8 to 6.0×10^8 Am^{-2} to study the static or DC characteristics of the device. Fig. 2 shows the static (i.e. when $m_x = 0$) electric field profiles of DDR diamond IMPATT for different bias current densities. It is observed from Fig. 2 that the electric field profiles are getting distorted due to the mobile space charge effect at higher bias current densities [36], [37]. The normalized current density profiles, i.e. $P(x)$-profiles of the device at different bias current densities are shown in Fig. 3. It is worthwhile to note that the $P(x)$-profile of the device smears out with the increase of bias current density. This indicates the sharp expansion of avalanche zone width x_A and consequent decrease in DC to RF conversion efficiency at higher bias current densities.

The important DC parameters such as peak electric field ξ_p, breakdown voltage V_B, avalanche voltage V_A, ratio of drift layer voltage to breakdown voltage V_D/V_B; where $V_D = V_B - V_A$, avalanche layer width x_A; where $x_A = |x_{A1}| + x_{A2}$, ratio of avalanche layer width to total drift layer width x_A/W; where $W = W_n + W_p$ of the device are obtained by taking the time averages of respective time varying parameters for different bias current densities and given in Tab. 2. Fig. 4 shows the variations of ξ_p, V_B and V_A with bias current density. It is observed from Tab. 2 and Fig. 4 that the peak electric field ξ_p decreases while both the breakdown voltage V_B and avalanche voltage V_A increase with the increase of bias current density J_0. The rate of increase of avalanche voltage with respect to bias current density (i.e. dV_A/dJ_0) is found to be larger than that of breakdown voltage (i.e. dV_B/dJ_0). That is why the ratio of drift zone voltage to breakdown voltage V_D/V_B decreases appreciably with bias current density J_0. The ratio of V_D/V_B is maximum (53.07%) at the bias current density J_0 of 3.0×10^8 Am^{-2}. The avalanche layer width x_A and the ratio of avalanche layer width to total drift layer width x_A/W increase from 0.534 to 1.027 µm and 35.59 to 68.47% respectively when the bias current density J_0 increases from 3.0×10^8 to 6.0×10^8 Am^{-2}.

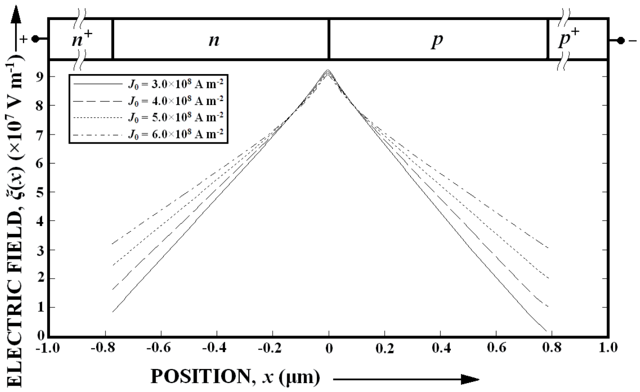

Fig. 2. Static electric field profiles for different bias current densities.

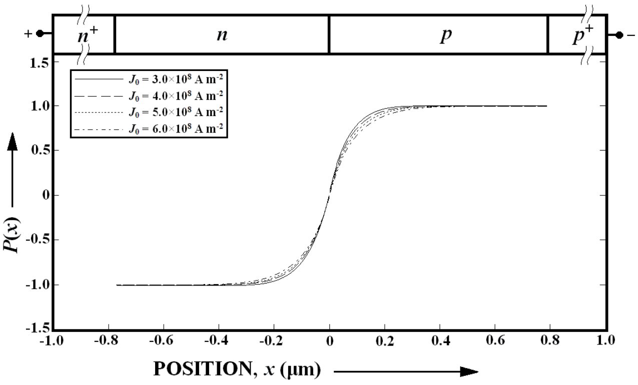

Fig. 3. Static $P(x)$-profiles for different bias current densities.

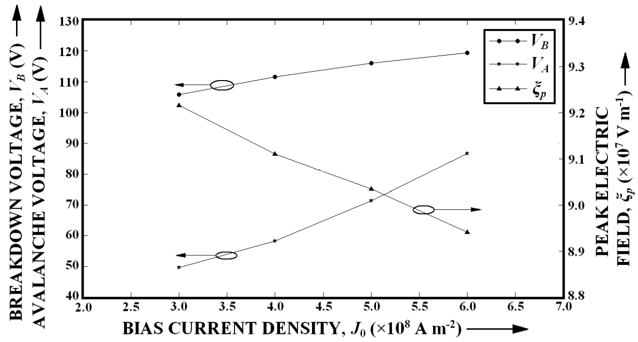

Fig. 4. Variations of peak electric field, breakdown voltage and avalanche voltage with bias current density.

PARAMETER	J_0 (A m^{-2})			
	3.0×10^8	4.0×10^8	5.0×10^8	6.0×10^8
ξ_p ($\times10^7$ V m^{-1})	9.2174	9.1118	9.0368	8.9431
V_B (V)	105.87	111.54	116.08	119.39
V_A (V)	49.69	58.33	71.34	86.64
V_D/V_B (%)	53.07	47.71	38.52	27.43
x_A (µm)	0.534	0.658	0.827	1.027
x_A/W (%)	35.59	43.88	55.18	68.47

Tab. 2. Static parameters.

3.2 Large-Signal Properties

Fig. 5 shows the diode voltage $V_B(t)$ and particle current $I_0(t) = J_0(t)\times A_j$ waveforms at different bias current densities for two consecutive cycles of steady-state oscillation taking 60% voltage modulation. Both the voltage and current waveforms are observed to be non-sinusoidal. The average values of diode voltage and particle current are found to be 105.87, 111.54, 116.08, 119.39 V and 288.6, 384.8, 481.1, 577.3 mA respectively. Further it is observed from Fig. 5 that the phase shift between the diode voltage and particle current is nearly 180^0, an essential condition for realizing maximum negative resistance and power from the device.

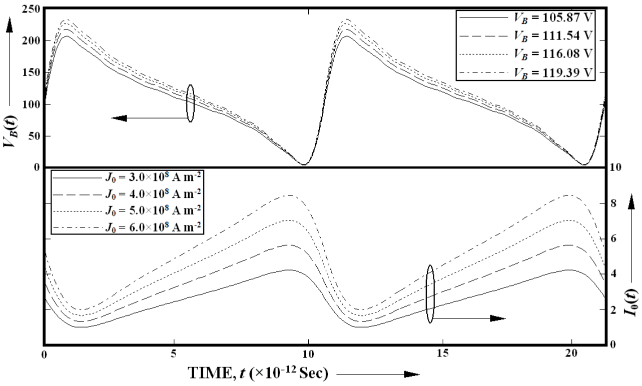

Fig. 5. Diode voltage and particle current waveforms at different bias current densities for two consecutive cycles of steady-state oscillation taking 60% voltage modulation.

The large-signal electric field snap-shots at quarter cycle intervals are shown in Fig. 6 (a) through (e) for five different phase angles at different bias current levels but at a fixed value of voltage modulation m_x = 60%. With increasing bias current density from 3.0×10^8 to 6.0×10^8 Am^{-2} and corresponding bias current from 288.6 to 577.3 mA, distortion and non-linearity is observed in the snap-shots at each phase angles $\omega t = 0$, $\pi/2$, π, $3\pi/2$, 2π. This is due to the mobile space charge effect at higher current densities [36]. [37]. The electric field snap-shots exhibit depletion width modulation at large-signal level for 60% voltage modulation (Fig. 6 (a) – (e)). This modulation changes both with time and bias current density. Higher depletion width modulation suggests higher punch through factor where punch through factor is defined as

$$PTF_n(t) = \frac{W_{Bn}(t)}{W_n} \quad \text{for } n\text{-side}, \tag{2}$$

$$PTF_p(t) = \frac{W_{Bp}(t)}{W_p} \quad \text{for } p\text{-side}, \tag{3}$$

where $W_{Bn}(t)$ and $W_{Bp}(t)$ are the depletion layer widths of n- and p-sides respectively at time t required for the electric field to be just punch through The punch through factors $PTF_n(t)$ and $PTF_p(t)$ for different bias current densities and phase angles, obtained from the large-signal electric field snap-shots are given in Tab. 3. It is observed from Tab. 3 that the punch through factor PTF is highest at $\omega t = \pi/2$ when the peak electric field is also highest and lowest at $\omega t = 3\pi/2$ when the peak electric field is lowest. This holds good for all bias current densities. But at a particular phase angle, $PTF(t)$ increases with increasing bias current density. This is due to the fact that the field distortion due to mobile space charges increases at higher bias current density.

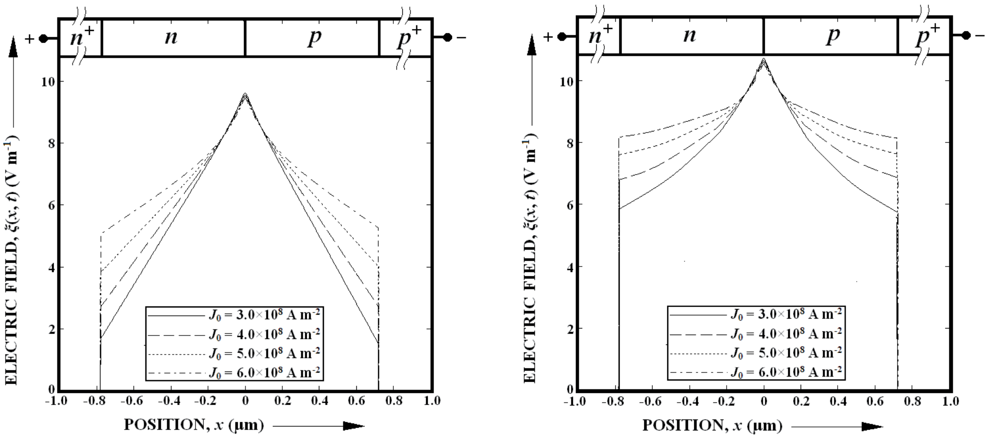

(a) $\omega t = 0$ (b) $\omega t = \pi/2$

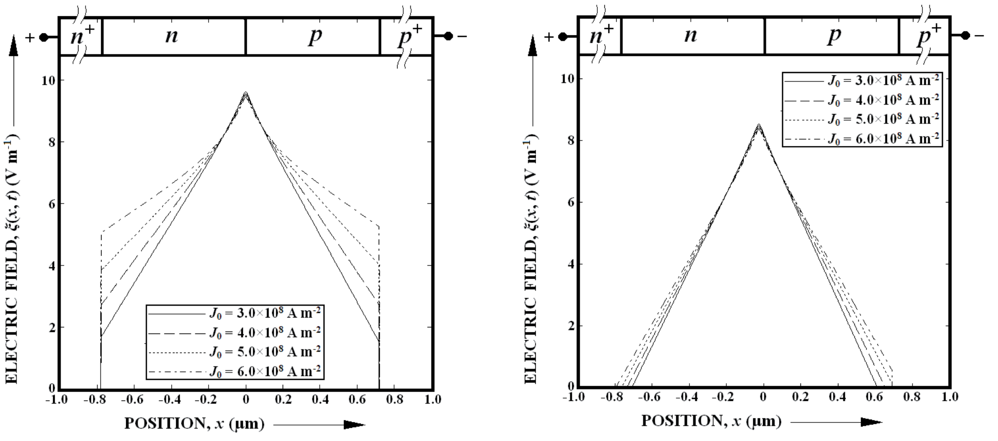

(c) $\omega t = \pi$

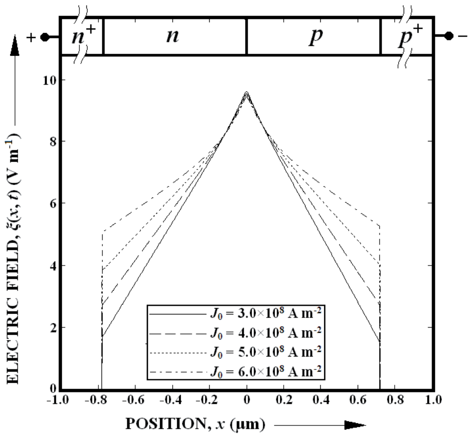

(e) $\omega t = 2\pi$

Fig. 6. Large signal electric field snap-shots at each quarter cycle of steady-state oscillation (a) $\omega = 0$, (b) $\omega = \pi/2$, (c) $\omega = \pi$, (d) $\omega = 3\pi/2$ and (e) $\omega = 2\pi$ for different bias current densities (voltage modulation is 60%).

J_0 ($\times 10^8$ A m^{-2})	$PTF_n(t)$ and $PTF_p(t)$ at different phase angles									
	$\omega t = 0$		$\omega t = \pi/2$		$\omega t = \pi$		$\omega t = 3\pi/2$		$\omega t = 2\pi$	
	$PTF_n(t)$	$PTF_p(t)$	$PTF_n(t)$	$PTF_p(t)$	$PTF_n(t)$	$PTF_p(t)$	$PTF_n(t)$	$PTF_p(t)$	$PTF_n(t)$	$PTF_p(t)$
3.0	1.0705	1.3194	3.0641	3.3194	1.0705	1.3194	0.8974	0.8403	1.0705	1.3194
4.0	1.4103	1.5556	4.7436	5.1389	1.4103	1.5556	0.9231	0.9028	1.4103	1.5556
5.0	1.6923	1.9167	5.8590	6.3472	1.6923	1.9167	0.9744	1.0278	1.6923	1.9167
6.0	2.5000	2.7778	9.1026	9.8611	2.5000	2.7778	1.0000	1.0694	2.5000	2.7778

Tab. 3. Punch through factors for different bias current densities at different phase angles.

Variations of peak negative conductance G_p and corresponding susceptance B_p with RF voltage V_{RF} considering the voltage modulation factor m_x from 5 to 70% for different bias current densities are shown in Fig. 7. The magnitude of G_p ($|G_p|$) decreases with the RF voltage V_{RF} for a particular bias current density and increases with the increase of bias current density for a particular RF voltage V_{RF}. On the other hand $|B_p|$ also decreases with the RF voltage V_{RF} for a particular bias current density and with increase of bias current density for a particular RF voltage V_{RF}.

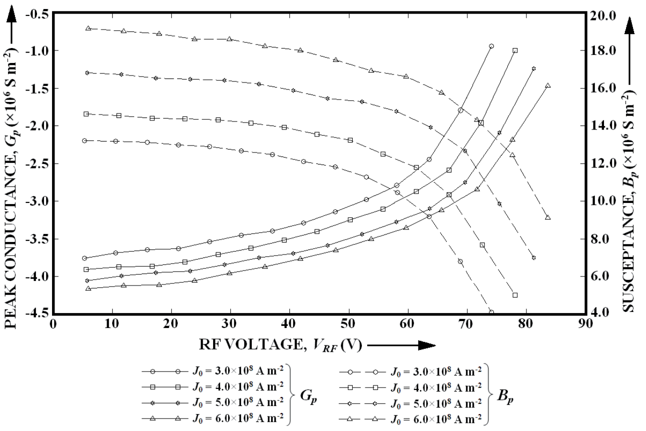

Fig. 7. Variations of peak negative conductance and corresponding susceptance with RF voltage at different bias current densities.

Fig. 8 shows the variations of optimum frequency f_p for peak negative conductance G_p and avalanche resonance frequency f_a (frequency at which device conductance just becomes negative) with RF voltage for different bias current densities. Both the optimum frequency f_p and avalanche resonance frequency f_a of the device decrease with the increase of RF voltage for a particular bias current density. But it is interesting to observe from Fig. 8 that the rate of decrease of optimum frequency with respect to RF voltage (i.e. df_p/dV_{RF}) is much sharper as compared to that of avalanche resonance frequency (i.e. df_a/dV_{RF}) for a particular bias current density. On the other hand both the optimum frequency f_p and avalanche resonance frequency f_a of the device increases with the increase of bias current density for a particular RF voltage.

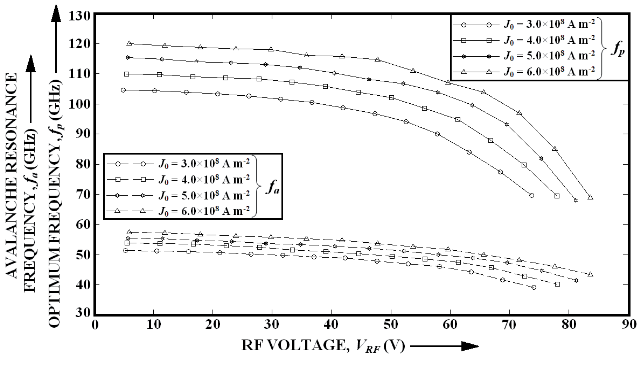

Fig. 8. Variations of avalanche resonance frequency and optimum frequency with RF voltage at different bias current densities.

The large-signal admittance characteristics of the device are shown in Fig. 9 for different bias current densities at 60% voltage modulation. The Q-factor $Q_p = -B_p/G_p$ of the device decreases from 3.79 to 5.08 when the bias current density increases from 3.0×10^8 to 6.0×10^8 Am^{-2} for $m_x = 60\%$.

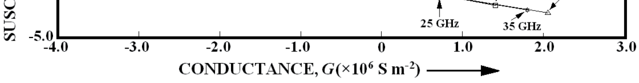

Fig. 9. Large-signal admittance characteristics of 94 GHz DDR diamond IMPATT for different bias current densities at 60% voltage modulation.

Fig. 10 shows the variations of RF power output $P_{RF} = (1/2)\times V_{RF}^2\times|G_p|\times A_j$; where $A_j = \pi(D_j/2)^2$ and large-signal DC to RF conversion efficiency $\eta_L = P_{RF}/P_{DC}$; where $P_{DC} = V_B\times J_0\times A_j$ with RF voltage for different bias current densities. It is interesting to observe that the RF power output increases initially with the increase of voltage modulation m_x attaining a peak at a value of $m_x = 60\%$ and then the same decreases for all current densities. The variations of large-signal efficiency η_L with RF voltage for all bias current densities are similar to that of P_{RF} with RF voltage. The results clearly indicate that the voltage modulation should be kept around 60% to obtain the optimum performance from the device. On the other hand RF power output P_{RF} of the device increases while large-signal DC to RF conversion efficiency η_L decreases with the increase of bias current density J_0 for a particular voltage modulation factor m_x. The maximum power output of 7.01 W with 10.18% DC to RF conversion efficiency is obtained from the device at a bias current density of 6.0×10^8 Am^{-2} and voltage modulation of 60%.

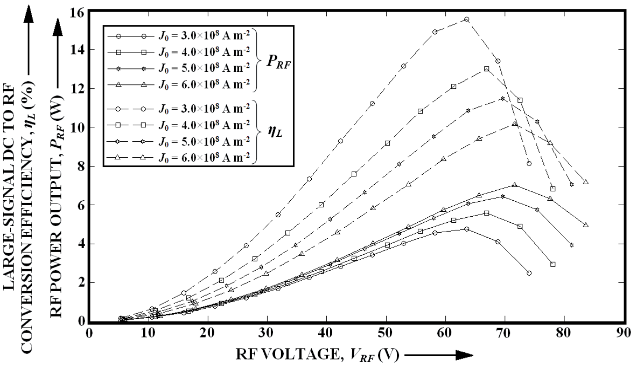

Fig. 10. Variations of RF power output and large-signal DC to RF conversion efficiency with RF voltage at different bias current densities.

3.3 Comparison with Experimental Results

The large-signal simulation of 94 GHz DDR Si IMPATT device which was reported by the authors in an earlier paper [25] show that the device is capable of delivering about 593 to 694 mW of power output with 7.45 to 8.74% conversion efficiency for 50 to 60% voltage modulation. Luy et al. [5] experimentally obtained maximum 600 mW of power output with 6.7% efficiency from 94 GHz DDR Si IMPATT fabricated using molecular-beam epitaxy (MBE) technique. Dalle et al. [6] reported experimental results of flat profile DDR Si IMPATT source at 94 GHz and they obtained about 500 mW of RF power output with 8.0% efficiency. Thus the experimental results are in very close agreement with the simulation results for DDR Si IMPATTs which validates the large-signal simulation technique developed by the authors and used in this paper. The large-signal simulation results presented in this paper indicate that 94 GHz DDR diamond IMPATT device can deliver 5.76 to 7.01 W peak RF power with 8.35 to 10.18% DC to RF conversion efficiency at a bias current density of 6.0×10^8 Am^{-2} and voltage modulation of 50 to 60%. This simulation study clearly indicates that the DDR diamond IMPATT excels DDR Si IMPATTs at millimeter-wave 94 GHz window frequency as regards power output and conversion efficiency. But so far as the authors' knowledge is concerned, no experimental report on the diamond based DDR IMPATT source is available in published literatures. That is why the simulation results presented in this paper could not be compared with experimentally obtained results.

4. Conclusions

Large-signal simulation is carried out in this paper to investigate the potentiality of DDR diamond IMPATT device as millimeter-wave source at 94 GHz window. Simulation results strongly established the fact that, diamond is an excellent base material for IMPATT devices at mm-wave frequencies. The simulation results and corresponding design would be useful for undertaking an experimental program to fabricate the 94 GHz DDR diamond IMPATTs by using microwave plasma-assisted chemical vapor deposition (MPCVD) followed by appropriate ion-implantation techniques.

References

[1] TREW, R. J., YAN, J. B., MOCK, P. M. The potentiality of diamond and SiC electronic devices for microwave and millimeter-wave power applications. *Proc. of IEEE*, 1991, vol. 79, no. 5, p. 598-620.

[2] MIDFORD, T. A., BERNICK, R. L. Millimeter wave CW IMPATT diodes and oscillators. *IEEE Trans. Microwave Theory Tech.*, 1979, vol. 27, no. 5, p. 483-492.

[3] CHANG, Y., HELLUM, J. M., PAUL, J. A., WELLER, K. P. Millimeter-wave IMPATT sources for communication applications. In *IEEE MTT-S International Microwave Symposium Digest*, 1977, p. 216-219.

[4] GRAY, W. W., KIKUSHIMA, L., MORENTC, N. P., WAGNER, R. J. Applying IMPATT power sources to modern microwave systems. *IEEE J. of Solid-State Circuits*, 1969, vol. 4, p. 409 - 413.

[5] LUY, J. F., CASEL, A., BEHR, W., KASPER, E. A 90-GHz double-drift IMPATT diode made with Si MBE. *IEEE Trans. Electron Devices*, 1987, vol. 34, p.1084-1089.

[6] DALLE, C., ROLLAND, P., LIETI, G. Flat doping profile double-drift silicon IMPATT for reliable CW high power high-efficiency generation in the 94-GHz window. *IEEE Trans Electron Devices*, 1990, vol. 37, p. 227-236.

[7] LUSCHAS, M., JUDASCHKE, R., LUY, J. F. Measurement results of packaged millimeter-wave silicon IMPATT diodes. In *Proc. of 27th International Conference on Infrared and Millimeter Waves, Conference Digest.* 2002, p. 135-136.

[8] LUSCHAS, M., JUDASCHKE, R., LUY, J. F. Simulation and measurement results of 150 GHz integrated silicon IMPATT diodes. *IEEE MTT-S International Microwave Symposium Digest*, 2002, p. 1269-1272.

[9] SHIH, H. D., BAYRAKTAROGLU, B., DUNCAN, W. M. Growth of millimeter-wave GaAs IMPATT structures by molecular beam epitaxy. *Journal of Vacuum Science & Technology B: Microelectronics and Nanometer Structures*, 1983, vol. 1, p. 199-201.

[10] EISELE, H., HADDAD, G. I. GaAs TUNNETT diodes on diamond heat sinks for 100 GHz and above. *IEEE Trans. Microwave Theory Tech.*, 1995, vol. 43, p. 210-213.

[11] MUKHERJEE, M., BANERJEE, S., BANERJEE, J. P. Dynamic characteristics of III-V and IV-IV semiconductor based transit time devices in the terahertz regime: A comparative analysis. *Terahertz Science and Tech.*, 2010, vol. 3, p. 98-109.

[12] MUKHERJEE, M., MAZUMDER, N. Optically illuminated 4H-SiC terahertz IMPATT device. *Egypt. J. Solids*, 2007, vol. 30, p. 87-101.

[13] MUKHERJEE, M., MAZUMDER, N., ROY, S. K. Prospects of 4H-SiC double drift region IMPATT device as a photo-sensitive high-power source at 0.7 terahertz frequency regime. *Active and Passive Electronic Components*, 2008, vol. 2008, p. 1-9.

[14] PANDA, A. K., PARIDA, R. K., AGARWALA, N. C., DASH, G. N. A comparative study on the high band gap materials (GaN and SiC) based IMPATTs. In *Proc. of Asia-Pacific Microwave Conference*. 2007, p 1-4.

[15] PANDA, A. K., PAVLIDIS, D., ALEKSEEV, E. DC and high-frequency characteristics of GaN-based IMPATTs. *IEEE Transaction on Electron Devices*, 2001, vol. 48, p. 820-823.

[16] BANERJEE, S., MUKHERJEE, M., BANERJEE, J. P. Bias current optimization of Wurtzite-GaN DDR IMPATT diode for high power operation at THz frequencies. *International Journal of Advanced Science and Technology*, 2010, vol. 16, p. 12-20.

[17] YUAN, L., JAMES, A., COOPER, J. A., MELLOCH, M. R., WEBB, K. J. Experimental demonstration of a silicon carbide IMPATT oscillator. *IEEE Electron Device Letter*, 2001, vol. 22, p. 266-268.

[18] VASSILEVSKI, K. V., ZORENKO, A. V., ZEKENTES, K., TSAGARAK,I K., BANO, E., BANC, C., LEBEDEV, A. 4H-SiC IMPATT diode fabrication and testing. In *Technical Digest of International Conference on SiC and Related Materials.* Tsukuba (Japan), 2001, p. 713-714.

[19] ACHARYYA, A., BANERJEE, J. P. Potentiality of IMPATT devices as terahertz source: An avalanche response time based approach to determine the upper cut-off frequency limits. *IETE Journal of Research*, accepted, publication schedule: March-April 2013.

[20] MOCK, P. M., TREW, R. J. Power generation of millimeter-wave diamond IMPATT diodes. In *Proc. of IEEE/Cornell Conference on Advanced Concepts in High Speed Semiconductor Devices and Circuits*. 1989, p. 383-389.

[21] HEWETT, C. A., ZEIDLER, J. R. Issues in diamond device fabrication. *Diamond and Related Materials,* 1991, p. 688-691.

[22] GURBUZ, Y., ESAME, O., TEKIN, I., KANG, W. P., DAVIDSON, J. L. Diamond semiconductor technology for RF device applications. *Solid-State Electronics*, 2005, vol. 49, p. 1055-1070.

[23] WILLANDER, M., FRIESEL, M., WAHAB, Q.U., STRAUMAL, B. Silicon carbide and diamond for high temperature device applications. *Journal of Materials Science: Materials in Electronics*, 2006, vol. 17, p. 1- 25.

[24] KASU, M. Diamond field-effect transistors as microwave power amplifiers. *NTT Technical Review*, 2010, vol. 8, no. 8, p. 1-5.

[25] ACHARYYA, A., BANERJEE, S., BANERJEE, J. P. Effect of junction temperature on the large-signal properties of a 94 GHz silicon based double-drift region impact avalanche transit time device. *Journal of Semiconductors*, vol. 34, no. 2, p. 024001-12.

[26] ACHARYYA, A., BANERJEE, S., BANERJEE, J. P. Large-signal simulation of 94 GHz pulsed DDR silicon IMPATTs including the temperature transient effect. *Radioengineering*, 2012, vol. 21, no. 4, p. 1218-1225.

[27] ACHARYYA, A., BANERJEE, S., BANERJEE, J. P. Temperature transient effect on the large-signal properties and frequency chirping in pulsed silicon DDR IMPATTs at 94 GHz. In *IEEE Conference CODEC 2012.* Institute of Radio Physics and Electronics, University of Calcutta, Kolkata, December 17-19, 2012, p. 133-136.

[28] ACHARYYA, A., BANERJEE, S., BANERJEE, J. P. A proposed simulation technique to study the series resistance and related millimeter-wave properties of Ka-Band Si IMPATTs from the electric field snap-shots. *International Journal of Microwave and Wireless Technologies*, 2013, vol. 5, no. 1, p. 91-100.

[29] SZE, S. M., RYDER, R. M. Microwave avalanche diodes. In *Proc. of IEEE, Special Issue on Microwave Semiconductor Devices*, 1971, vol. 59, p. 1140-1154.

[30] KONOROVA, E. A., KUZNETSOV, Y. A., SERGIENKO, V. F., TKACHENKO, S. D., TSIKUNOV, A. K., SPITSYN, A. V., DANYUSHEVSKI, Y. Z. Impact ionization in semiconductor structures made of ion-implanted diamond. *Sov. Phys. – Semicond.*, 1983, vol. 17, p. 146-149.

[31] FERRY, D. K. High-field transport in wide-bandgap semiconductors. *Phys. Rev. B*, 1975, vol. 12, p. 2361-2369.

[32] CANALI, C., GATTI, E., KOZLOV, S. F., MANFREDI, P. F., MANFREDOTTI, C., NAVA, F., QUIRINI, A. Electrical properties and performances of neutral diamond nuclear radiation detectors. *Nuclear Instrum. and Methods*, 1979, vol. 160, p. 73-77.

[33] OSMAN, M. A., ANDREWS, G., KRESKOVSKY, J. P., GRUBIN, H. L. Numerical simulation studies of semiconducting diamond electronic devices. *Final Report on Contract DNA001-87-C-0250, Defense Nuclear Agency*, 1989.

[34] NAVA, F., CANALI, C., JACOBONI, C., REGGIANI, L., KOZLOZ, S. F. Electron effective masses and lattice scattering in neutral diamond. *Solid State Commun.*, 1980, vol. 33, p. 475-477.

[35] Electronic Archive: *New Semiconductor Materials, Characteristics and Properties*, 2012. [Online] Available at: http://www.ioffe.ru/SVA/NSM/Semicond/Diamond/index.html.

[36] SRIDHARAN, M., ROY, S. K. Computer studies on the widening of the avalanche zone and decrease on efficiency in silicon X-band symmetrical DDR. *Electron Lett.*, 1978, vol. 14, p. 635-637.

[37] SRIDHARAN, M., ROY, S. K. Effect of mobile space charge on the small signal admittance of silicon DDR. *Solid State Electron*, 1980, vol. 23, p. 1001-1003.

About Authors...

Aritra ACHARYYA was born in 1986 at Serampore, W. B., India. He received his M.Tech. degree Radio Physics and Electronics from the Institute of Radio Physics and Electronics, University of Calcutta, Kolkata, India. Earlier he obtained his B. E. degree in Electronics and Telecommunication Engineering from Bengal Engineering and Science University (BESU), Shibpur, Howrah, W.B., India. Presently he is pursuing his Ph.D. from University of Calcutta under Professor (Dr.) J. P. Banerjee, Radio Physics and Electronics Department, C.U., Kolkata, India. He joined the Department of Electronics and Communication Engineering, Supreme Knowledge Foundation Group of Institutions, Sir J. C. Bose School of Engineering, Mankundu, Hooghly, W. B., India in 2010 as a lecturer. Presently he is working as an assistant professor in the same institution since 2011. He is the recipient of Pareshlal Dhar Bhowmik book award in the year 2010 for securing highest marks in M.Tech. (Radio Physics and Electronics) examination 2010 of University of Calcutta. His research interest is millimeter-wave and terahertz semiconductor devices and their optical control. He is the principle coauthor of more than 50 research papers in different national and international journals and conference proceedings.

Koyel DATTA was born in 1991. Presently she is pursuing B.Tech. in Electronics & Communication Engineering from Supreme Knowledge Foundation Group of Institutions, Sir J. C. Bose School of Engineering, Mankundu, Hooghly, W. B., India. Her area of interest is wide bandgap (WBG) semiconductor based millimeter-wave and terahertz sources.

Raya GHOSH was born in 1991. Presently she is pursuing B.Tech. in Electronics & Communication Engineering from Supreme Knowledge Foundation Group of Institutions, Sir J. C. Bose School of Engineering, Mankundu, Hooghly, W. B., India. Her area of interest is wide bandgap (WBG) semiconductor based millimeter-wave and terahertz sources.

Monalisa SARKAR was born in 1992. Presently she is pursuing B.Tech. in Electronics & Communication Engineering from Supreme Knowledge Foundation Group of Institutions, Sir J. C. Bose School of Engineering, Mankundu, Hooghly, W. B., India. Earlier she obtained diploma in Electronics and Telecommunication Engineering from Women's Polytechnic, Chandannagar, Hooghly, W. B., India in the year 2010. Her area of interest is wide bandgap (WBG) semiconductor based millimeter-wave and terahertz sources.

Roshmy SANYAL was born in 1989. Presently she is pursuing B.Tech. in Electronics & Communication Engineering from Supreme Knowledge Foundation Group of Institutions, Sir J. C. Bose School of Engineering, Mankundu, Hooghly, W. B., India. Earlier she obtained diploma in Electronics and Telecommunication Engineering from Women's Polytechnic, Chandannagar, Hooghly, W. B., India in the year 2010. Her area of interest is wide bandgap (WBG) semiconductor based millimeter-wave and terahertz sources.

Suranjana BANERJEE was born in 1980. She received her B.Sc. (Hons.) degree in Electronics Science in 2002 from the University of Calcutta, India and topped the merit list. She received her B.Tech and M.Tech. degrees from the Institute of Radio Physics and Electronics, University of Calcutta, Kolkata, India in 2005 and 2008 respectively. Presently she has been working as Assistant Professor in Academy of Technology, an Engineering college at Adisaptagram, Hooghly 712121, W. B., India under West Bengal University of Technology. She has been carrying out research work in the area of both homo-junction and hetero-junction ATT devices under CW and pulsed operations at millimeter wave and terahertz frequency bands. She has published a number of research papers in referred journals and conference proceedings.

Professor (Dr.) J. P. BANERJEE was born in 1947. He obtained B.Sc. (Hons.) and M.Sc. in Physics and Ph.D. in Radio Physics and Electronics from University of Calcutta. He worked as a senior scientist of the Department of Electronics project in the Institute of Radio Physics and Electronics, C.U. during 1986-1989. He joined the Department of Electronic Science, C.U. in 1989 as a reader. He has been working as a professor in the Institute of Radio Physics and Electronics, C.U. since 1998. He is the recipient of the Indian National Science Academy Award of a visiting fellowship and Griffith Memorial Prize in Science of the Calcutta University in 1986. He is the principle co-author of more than 150 research papers in international journals in the fields of Semiconductor Science and Technology, Microwave and Millimeter wave avalanche transit time devices and avalanche Photo Detectors. He has successfully carried out a number of research projects of Government of India on IMPATT diodes. A collaborative research work in the field of computer analysis, fabrication and characterization of V-Band silicon double-low-high-low IMPATTs was successfully carried out by Dr. Banerjee for the first time with Dr. J. F. Luy the eminent German scientist of Daimler Benz Research Centre. He is a fellow of the Inst. of Electronics and Telecommunication Engineers (IETE), a life member of society of EMI and EMC and Semiconductor Society, India. He is an expert committee member of All India Council of Technical Education (AICTE) and served as a referee for various technical journals.